ACS Partner Journal

CHEM & BIO ENGINEERING



pubs.acs.org/ChemBioEng

Article

# Harnessing Solar-Salinity Synergy with Porphyrin-Based Ionic Covalent-Organic-Framework Membranes for Enhanced Ionic Power Generation

Weipeng Xian,[#] Changjia Zhu,[#] Zhuozhi Lai, Qing Guo, Di Wu, Qing-Wei Meng, Sai Wang, Shengqian Ma, and Qi Sun*

Cite This: *Chem Bio Eng.* 2024, 1, 461−468

Read Online

ACCESS | Metrics & More | Article Recommendations | Supporting Information

**ABSTRACT:** Nature seamlessly integrates multiple functions for energy conversion, utilizing solar energy and salinity gradients as the primary drivers for ionic power generation. The creation of artificial membranes capable of finely controlling ion diffusion within nanoscale channels, driven by diverse forces, remains a challenging endeavor. In this study, we present an innovative approach: an ionic covalent-organic framework (COF) membrane constructed using chromophoric porphyrin units. The incorporation of ionic groups within these nanoconfined channels imparts the membrane with exceptional charge screening capabilities. Moreover, the membrane exhibits photoelectric responsivity, enhancing the ion conductivity upon exposure to light. As a result, this leads to a substantial increase in the output power density. In practical terms, when subjected to a salinity gradient of 0.5/0.01 M NaCl and exposed to light, the device achieved an outstanding peak power density of 18.0 ± 0.9 W $m^{-2}$, surpassing the commercial benchmark by 3.6-fold. This innovative membrane design not only represents a significant leap forward in materials science but also opens promising avenues for advancing sustainable energy technologies.

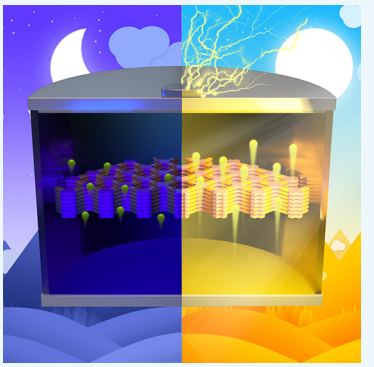

**KEYWORDS:** *covalent-organic-framework membrane, opto-ionic effect, solar-salinity synergy, reverse electrodialysis, sustainable energy harvesting*



## INTRODUCTION

The objective of the Paris Agreement, aimed at limiting global warming to below 2 °C, has encountered skepticism regarding the feasibility of reducing anthropogenic greenhouse gas emissions at a sufficient rate. Consequently, there has been a growing impetus to explore alternative energy sources capable of facilitating the transition to a net-zero carbon emissions future. The pursuit of a more sustainable global energy portfolio offers a promising avenue to tackle this challenge.[1] Among the various alternatives, solar energy and salinity gradient energy have emerged as particularly promising options.[2−10] However, technologies that could concurrently harness these energy sources remain relatively untapped. In the domain of classical physics, the discipline of ionics presents a captivating counterpart to electronics. It opens avenues for integrating the capabilities of ionic membranes with the unique attribute of light responsiveness, thereby creating a promising amalgamation of functionalities.[11,12] The major scientific challenge in this endeavor is developing ionic membranes that also exhibit photoelectric effects (Figure 1).[11,12] To date, the development of ionic materials with photoelectric properties is in its infancy, with only a few studies conducted in this area.[26,27] To successfully bridge this gap, membranes with the following attributes are highly desired: (1) amenable synthesis to enable the integration of multiple functionalities, (2) conjugated structures constructed by chromophores to boost the photoelectric responsivity upon light absorption, and (3) abundant ionic nanochannels to achieve high permselectivity and provide efficient transport pathways.

Covalent organic frameworks (COFs) have emerged as a promising class of crystalline porous materials with customizable characteristics for various applications.[28−36] Their modular nature allows for the assembly of building blocks from a wide range of organic molecules and subsequent post-synthetic modification of pore channels with specific functional groups. Notably, COFs offer the flexibility to integrate chromophores as building units and attach ionic entities to the pore walls, making them well-suited for the creation of ionic materials with photoelectric responsiveness.[37−43] Furthermore, two-dimensional COFs (2D COFs) distinguish themselves for their unique advantages in membrane

**Received:** December 20, 2023
**Revised:** March 21, 2024
**Accepted:** March 22, 2024
**Published:** May 8, 2024

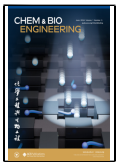

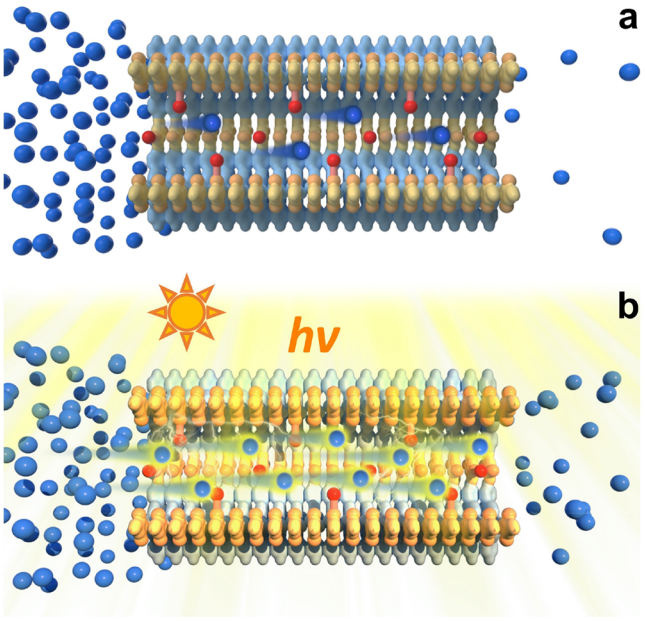


**Figure 1.** Schematic representation of the integration of ionic membranes (a) with light responsiveness (b). This diagram illustrates the functional interconnection between the consolidated ionic membranes (highlighted by red spheres representing ionic sites) and the responsiveness to light, resulting in a synergistic enhancement of the ion transport.

fabrication, aligning with the pursuit of this innovative goal.[44−57] The conjugated 2D layers often adopt eclipsed configurations, facilitating charge carrier migration. Simultaneously, the continuous 1D channels serve as conduits for ion mobility, enhancing the potential for synergistic energy conversion.

Porphyrin was chosen as a chromophore strut to illustrate this concept due to its proven efficiency in light-harvesting and electron-transfer processes in both natural and artificial systems.[58−65] Ionic groups were introduced to the COFs by combining a hydroxy-functionalized monomer with the porphyrin unit for additional chemical modifications. The resulting membranes undergo efficient charge separation when exposed to light, generating a transmembrane electric field that directs ion movement across the membrane. The photogating activity could be finely and reversibly adjusted by varying the light intensity. Additionally, the decorated ionic sites impart the membrane with ionic screening capabilities, showing outstanding permselectivity across various salt concentration gradients. These features point to its immense potential in converting ionic energy to electricity. Remarkably, the multifunctional membrane yielded a power density of up to $10.8 \pm 0.5$ W m$^{-2}$ in the reverse electrodialysis (RED) mode at the mimic estuary conditions (0.5/0.01 M NaCl). When illuminated by a xenon lamp, this value surged to $18.0 \pm 0.9$ W m$^{-2}$, approximately quadrupling the standard commercial benchmark of 5 W m$^{-2}$.[13−25] This work represents one of the pioneering efforts in constructing ionic membranes with a photoelectronic effect. The versatility of COFs in developing multifunctional membranes underscores their immense potential for sustainable energy utilization and integration into next-generation devices.

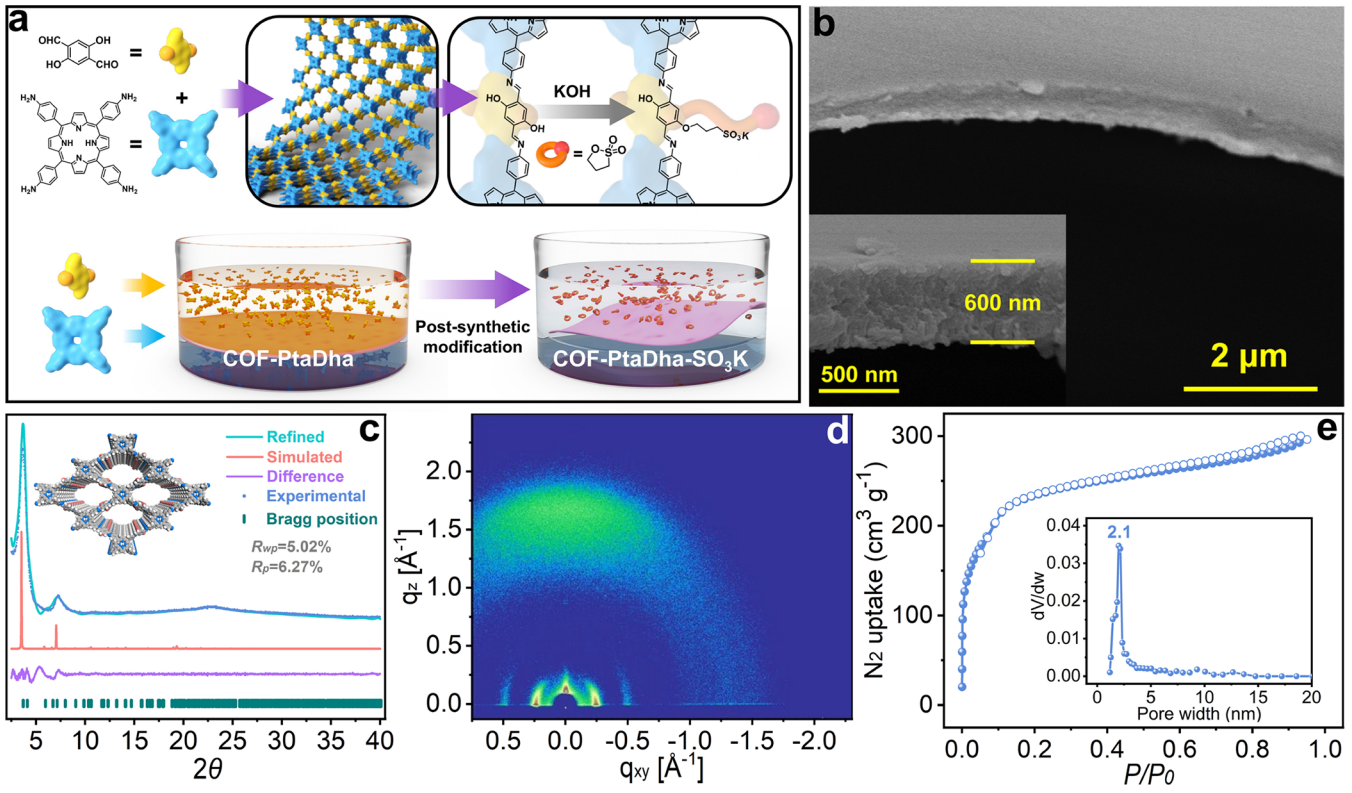


**Figure 2.** Synthesis and characterization of COF-PtaDha. (a) Synthetic scheme of the free-standing COF membrane (COF-PtaDha) via interfacial polymerization and the subsequent post-synthetic modification with 1,3-propane sultone to yield COF-PtaDha-$SO_3K$, and (b) SEM images (inset, a cross-section areal SEM image), (c) XRD patterns (inset, graphic view of AA stacking structure), (d) GIWAXS pattern, and (e) $N_2$ sorption isotherm collected at 77 K (inset, pore size distribution).



https://doi.org/10.1021/cbe.3c00119
Chem Bio Eng. 2024, 1, 461−468

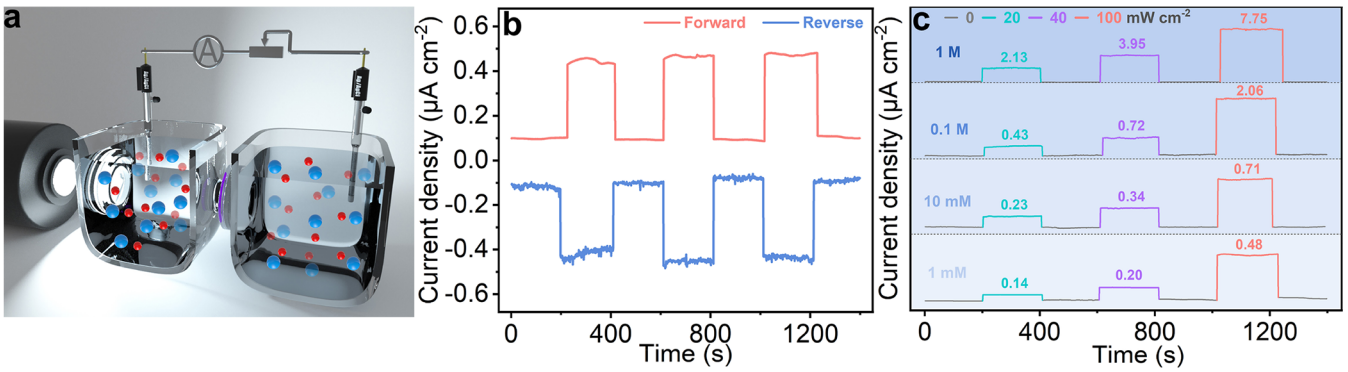


**Figure 3.** Light-controlled ionic responses of COF-PtaDha. (a) Schematic of the experimental setup. COF-PtaDha exhibits the photo-induced ionic flow directing from illuminated to unilluminated sides. (b) Current−time characteristics of the device measured in the absence of light and under illumination (100 mW $cm^{-2}$) with varying light directions. The two quartz compartments are filled with 0.1 M KCl aqueous solutions. "Forward" and "reverse" denote the direction of light incidence, with "forward" indicating light incident on the membrane facing the organic phase and "reverse" indicating light incident on the membrane facing the aqueous phase during synthesis. (c) Current−time curves upon illumination with various intensities of xenon lamp measured at different equimolar concentrations of KCl aqueous solutions spanning a range of 1 mM to 1 M.

## RESULTS AND DISCUSSION

**Membrane Preparation and Characterization.** We developed a free-standing porphyrin-based COF membrane, denoted as COF-PtaDha, through an acetic acid-catalyzed Schiff-base condensation reaction under interfacial polymerization conditions. This process involved combining an acetic acid aqueous solution of 4,4′,4″,4‴-(porphyrin-5,10,15,20-tetrayl)tetraaniline (Pta) with an ethyl acetate-mesitylene 2,5-dihydroxyterephthalaldehyde (Dha) solution (Figure 2a). The Fourier transform infrared (FT-IR) analysis of COF-PtaDha revealed a distinctive peak at 1602 $cm^{-1}$, indicating the presence of C═N stretching vibrations. Remarkably, the peaks corresponding to the $NH_2$ and CHO groups of the monomers, initially at 3273 and 1641 $cm^{-1}$, respectively, were significantly reduced, implying a high degree of polymerization within the membrane (Figure S1). To further validate the formation of COFs, solid-state $^{13}C$ nuclear magnetic resonance (NMR) spectroscopy was employed. The appearance of a C═N signal at 162.0 ppm in the NMR spectrum (Figure S2) provided strong evidence for the successful formation of the COF structure.[65] Scanning electron microscopy (SEM) was utilized to examine the surface morphology of the membrane, revealing a defect-free structure. This observation indicates that ion transport occurs exclusively through the inherent pores within the COF membrane (Figure 2b and Figure S3). A closer inspection of the cross-sectional morphology, via SEM, revealed a compact arrangement with a thickness close to 600 nm (Figure 2b, inset). The powder X-ray diffraction (PXRD) pattern of the free-standing COF-PtaDha membrane exhibited sharp reflections, suggesting the formation of a highly crystalline material (Figure 2c). The crystal structure was confirmed by comparing the experimental data with the simulated pattern of PBAN arrangement, showing excellent agreement (Figure 2c, inset, Figure S4, and Table S1). Two-dimensional grazing-incidence wide-angle X-ray scattering (GIWAXS) measurements confirmed the crystalline nature and strong texture of the COF membrane. Notably, the *hk*0 reflections exhibited peak intensity near the horizon of the membrane, indicating a predominant orientation of the *a*−*b* plane. This orientation is advantageous, as it ensures that the COF pores, aligned parallel to the transport direction, remain unobstructed (Figure 2d). The Brunauer−Emmett−Teller (BET) surface area of the free-standing COF-PtaDha membrane, derived from $N_2$ sorption isotherms, was calculated to be 775 $m^2$ $g^{-1}$, with a pore size distribution centered at 2.1 nm. These findings align well with the expected characteristics of the proposed structure (2.1 nm; Figure 2e). To explore the light-absorption properties of the COF-PtaDha membrane, ultraviolet−visible (UV−vis) spectroscopy was employed, revealing a strong absorbance over the UV−vis spectral range, showing outstanding light-absorption behavior. The optical bandgap, derived from the corresponding Tauc plot, was estimated to be 1.46 eV (Figure S5).[66] These attributes underscore the significant potential of COF-PtaDha for applications in light-driven ion transport.

**Investigation of the Opto-ionic Effect of the Membrane.** We subsequently embarked on an exploration of the capabilities of COF-PtaDha in facilitating ion transport under illumination. To enhance operability, we affixed the COF-PtaDha membrane onto a polyacrylonitrile (PAN) ultrafiltration membrane due to its optical transparency and flexibility. The light-modulated ionic transport characteristics of COF-PtaDha were investigated by using a custom-made conductive cell. In this setup, we positioned the membrane between two quartz compartments, both filled with identical solutions of aqueous KCl (Figure 3a). To investigate the photoresponsiveness of the resulting device, current−time (*I*−*t*) traces were collected under alternating light-on and -off conditions, using a pair of lightproof shield-protected Ag/AgCl electrodes (Figure S6). In the absence of light irradiation, the system maintained a steady state, with minimal electron flow through the external circuit, attributed to the disparate diffusion of $K^+$ and $Cl^-$ ions.[67] Upon illumination of the membrane, an instantaneous photoionic response became apparent in the *I*−*t* trace, maintaining stability under prolonged irradiation and reverting to its initial state upon the cessation of light exposure. Altering the direction of illumination on the membrane leads to a reversal of the generated electric current (Figure 3b). One of the notable findings was the strong correlation between the amplitude of the photocurrent and both the light intensity of xenon lamps and the concentration of KCl. Specifically, a photocurrent density of up to 7.75 μA $cm^{-2}$ was achieved in a 1 M KCl environment under the irradiation of a 100 mW $cm^{-2}$ xenon lamp. This magnitude was notably 93 times greater than that observed under dark conditions (Figure 3c and Figure S7). To


https://doi.org/10.1021/cbe.3c00119
Chem Bio Eng. 2024, 1, 461−468

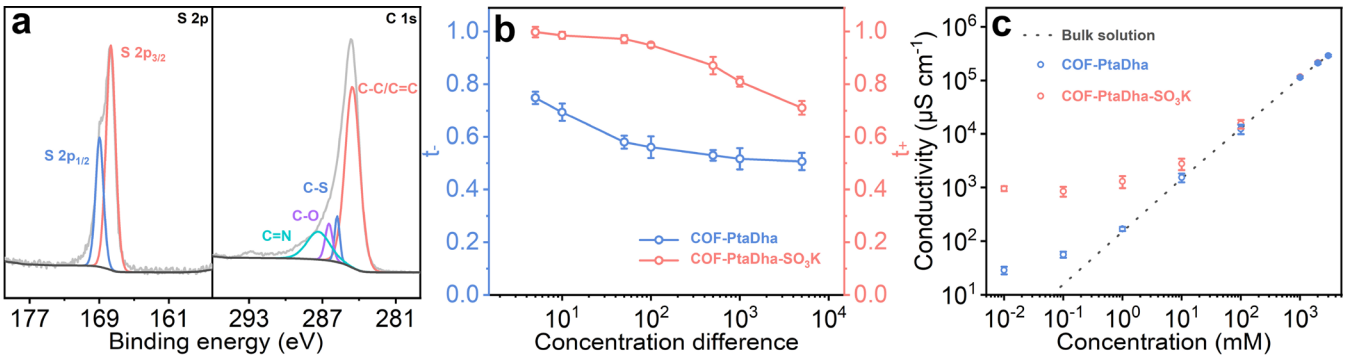


**Figure 4.** Characterization and ionic transport properties of COF-PtaDha-$SO_3K$. (a) XPS profiles. (b) Plots of the transference numbers ($t$) versus various KCl concentration differences, whereby the low-concentration side is set as 0.1 mM. (c) Conductivity versus KCl concentration. The ionic conductivity deviates from the bulk value (dashed line) in the low-concentration region, suggestive of surface-charge governed ion transport.

investigate the impact of light wavelength on the intensity of the light-induced ionic current, we observed that the order of response was as follows: blue > white > green > red LED lamp. This sequence corresponds to the maximum-absorption wavelength observed in the UV−vis spectrum of the COF-PtaDha membrane (Figure S8).

The observed photogating effects are believed to result from changes in the driving force for ion transport triggered by light. These effects can be explained by the concept of the photoelectric effect, encompassing both photovoltaic (generation of electric voltage) and photoconductive (change in conductivity) effects. To uncover the underlying mechanism, we investigated the photo-induced transmembrane voltage changes at various KCl concentrations. Interestingly, we found that as the KCl concentration increases, the magnitude of the photovoltage decreases, which contradicts the correlation between the phototriggered ionic current and KCl concentration. This suggests that the increase in the ionic current is not dependent on the generated photovoltage and can be best explained by the photoconductive effect. When the COF-PtaDha membrane is illuminated, light stimulates the generation of photoexcited electrons and holes. These charge carriers are capable of migrating within the membrane and engaging with ions, thereby facilitating ion transport. Increasing the power density of the Xe lamp amplifies the photochemical reaction, resulting in the generation of a greater number of charge-separated entities. Consequently, this reduces the energy required for ion movement across the membrane, leading to an augmentation in photo-induced ionic current (Figure 3c). Furthermore, a discernible linear correlation between light intensity and photo-induced ionic current was established (Figure S9). To support this explanation, we conducted conductance tests under varying light conditions, revealing a clear disparity between the current−voltage ($I$−$V$) curves obtained under external light and those acquired in darkness, confirming the generation of additional surface charge when the membrane is exposed to light (Figure S10).

Given the significance of temperature gradients in influencing ion transport, we conducted temperature measurements between the two quartz compartments during our experiments to assess the potential impact of heat-induced changes in conductivity. Our measurements revealed a maximum temperature gradient of 3.5 °C (Figure S11). To further investigate this effect, we tested the system with a larger temperature gradient of 5 °C between the compartments and found that the resulting $I$−$V$ curve closely matched the original curve. This observation suggests that the temperature increases induced by light in the solution do not substantially alter its conductivity (Figure S12). Although exposure to light did lead to a slight temperature increase in the COF-PtaDha membrane due to its photothermal effect, increasing from 23.3 to a peak of 26.8 °C within 20 s before stabilizing (Figure S13), we can effectively exclude the impact of this light-triggered membrane heating. This conclusion arises from the consideration that the axial temperature gradient resulting from the membrane's heating would drive ion transport in a direction opposite to what was observed in the photocurrent. Therefore, the temperature gradient created by light-induced heating does not play a dominant role in terms of explaining the observed current response.

**Photoresponsive Ionic Membrane Preparation and Characterization.** To confer charge screening capabilities upon the COF-PtaDha membrane, we conducted a series of post-synthetic modifications. Initially, the membrane was treated with an ethanol solution of potassium hydroxide, followed by a subsequent reaction with 1,3-propane sultone. This chemical process resulted in the attachment of alkyl chains featuring terminal potassium-sulfonate groups (−$SO_3K$) onto the pore channels, with the resulting membrane denoted as COF-PtaDha-$SO_3K$ (Figure 2a). To assess the success of these modifications, various analytical techniques, including FT-IR and X-ray photoelectron spectroscopy (XPS), were employed. The verification of post-modification was established by observing additional peaks at 1210 and 1035 $cm^{-1}$ in the IR spectrum of the COF-PtaDha-$SO_3K$ membrane, corresponding to the S═O stretching vibration (Figure S14).[62] The presence of sulfur signals, specifically S $2p_{1/2}$ at 169.5 eV and S $2p_{3/2}$ at 167.7 eV, in the XPS profile of the COF-PtaDha-$SO_3K$ membrane, provided further evidence confirming the presence of sulfonate anions (Figure 4a). Moreover, the content of ionic sites on the COF-PtaDha-$SO_3K$ membrane was estimated to be approximately 1.19 mmol $g^{-1}$ based on the relative integral area of the C−S bond in the XPS spectrum of C 1s. SEM images visually confirmed the intact morphology of the membrane after the post-synthetic modification process (Figure S15). Additionally, the PXRD pattern of the COF-PtaDha-$SO_3K$ membrane closely resembled that of the COF-PtaDha, affirming the retention of the crystalline structure (Figure S16). The BET surface area of the COF-PtaDha-$SO_3K$ membrane, was determined to be 85 $m^2$ $g^{-1}$, showcasing a decrease compared to the pristine


https://doi.org/10.1021/cbe.3c00119
Chem Bio Eng. 2024, 1, 461−468

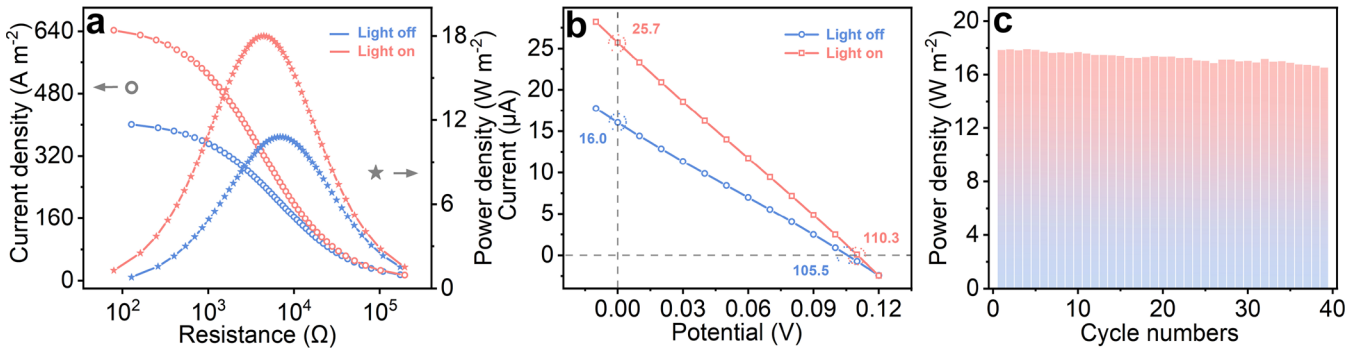


**Figure 5.** Solar-salinity synergy of COF-PtaDha-$SO_3K$ and stability of the corresponding RED device. (a) Power output to an external circuit supplying an electronic load for COF-PtaDha-$SO_3K$ before and after illumination under a 100 mW $cm^{-2}$ xenon lamp, along with the corresponding variation of diffusion current. The two quartz compartments were filled with 0.01 and 0.5 M NaCl aqueous solutions, respectively. The resistance of COF-PtaDha-$SO_3K$ decreased upon illumination. (b) $I-V$ plots for COF-PtaDha-$SO_3K$ recorded in 0.01/0.5 M NaCl concentration difference before and after illumination. (c) Cycle series of the output power density of the RED device recorded in 0.01/0.5 M NaCl concentration difference under the illumination of a 100 mW $cm^{-2}$ xenon lamp.

membrane. This reduction is attributed to the additional mass introduced during the post-modification process (Figure S17).

To assess the permselectivity of COF-PtaDha-$SO_3K$, we collected $I-V$ curves under varying KCl concentration gradients. One compartment maintained a constant KCl concentration of 0.1 mM, while the other compartment experienced an increase from 0.5 mM to 0.5 M (Figure S18). An investigation into the impact of introduced ionic sites was conducted by comparing the permselectivities of COF-PtaDha and COF-PtaDha-$SO_3K$. Figure 4b illustrates the transference numbers ($t$) for both COF-PtaDha and COF-PtaDha-$SO_3K$, plotted against the concentration difference. Notably, COF-PtaDha exhibited minimal charge selectivity, with $t$ values approaching 50% even at a concentration difference of 50. On the contrary, the incorporation of negative potassium-sulfonate groups into COF-PtaDha markedly improved its permselectivity, reversing it from anion selectivity to cation selectivity. The permselectivity approached 1 for salt concentration disparities below 50 and remained at 0.82, even at a concentration differential of 1000.

To comprehend the origin of the charge selectivity of COF-PtaDha-$SO_3K$, we measured ion conductance by exposing the membrane to equimolar KCl solutions spanning concentrations from 0.01 mM to 3 M. Plotting conductance against KCl concentration revealed a notable deviation of transmembrane conductance from the bulk value (represented by the dashed line) at KCl concentrations below 10 mM (Figure 4c and Figure S19). This suggests that under these specific conditions, ion transport is predominantly governed by surface charge effects. Transmembrane conduction approximated bulk values as KCl concentrations increased, which is attributed to the diminishing influence of the electric double layer (EDL) at higher salt concentrations, thereby weakening the surface-charge-dependent ion transport (Table S2).

**Enhancing Ionic Power Generation through Solar-Salinity Synergy.** The exceptional permselectivity and opto-ionic effects of COF-PtaDha-$SO_3K$ have led to exploration of its use in ionic power generation via solar-salinity synergy. To mimic the salinity gradients commonly found in estuaries, we employed NaCl solutions with concentrations of 0.5 and 0.01 M. This choice is driven by the fact that each cubic meter of seawater and river water contains a substantial energy reserve of up to 2.3 MJ. Reversed electrodialysis (RED) stands out as a well-established and effective method for converting ionic power into electricity. The power generated through this process can be effectively harnessed by utilizing external load resistors ($R_L$). As depicted in Figure 5a, we observe how the diffusion current decreases with increasing resistance ($R_L$), ultimately reaching its peak value of 10.8 ± 0.5 W $m^{-2}$ at a resistance value of 7 kΩ. Taking into account the previously mentioned opto-ionic effects, we anticipated that light-induced electrons would synergize with the $-SO_3K$ groups, facilitating cation transport and thereby enhancing ion selectivity and conductivity. Indeed, upon exposure to light (as demonstrated in Figure 5b), there were noticeable enhancements in both the open-circuit voltage ($V_{oc}$) and the short-circuit current ($I_{sc}$). As a result, the power density was determined to be 1.7 times greater than in the absence of light, surpassing the performance of most advanced membrane technologies currently available (as detailed in Table S3). Furthermore, under illumination, the resistance of the COF-PtaDha-$SO_3K$ decreased to 4 kΩ (Figure 5b). These findings indicate that the output power density of RED can be significantly increased during daylight hours by directing sunlight onto the membranes. To elucidate the role of PAN in the generated output power density, we evaluated its performance. Our analysis revealed that the output power density generated solely by PAN accounts for only 1.4% of the total output power density of COF-PtaDha-$SO_3K$/PAN, highlighting the negligable contribution of the PAN membrane to the overall output power density (Figure S20). Furthermore, the RED system exhibited remarkable stability, consistently outputting nearly 40 cycle series, thereby showcasing promising prospects for practical applications (Figure 5c).

## ■ CONCLUSION

In summary, this study has showcased a conceptual demonstration of novel photoresponsive ionic membranes optimized for superior ionic power generation. Our findings underscore the profound influence of opto-ionic effects in amplifying ion conductivity and diminishing membrane resistance. This culminates in a marked enhancement of the power density of the RED device. This study illuminates the synergistic interplay of various components in energy transduction at the nanoscale within synthetic structures, heralding a new frontier for innovative and practical applications. Additionally, the adaptability of COF materials underscores a promising avenue for multifunctional integration, heralding


https://doi.org/10.1021/cbe.3c00119
Chem Bio Eng. 2024, 1, 461−468

exhilarating opportunities for future scientific exploration and technological breakthroughs.

## EXPERIMENTAL SECTION

**Fabrication of the Free-Standing COF-PtaDha Membrane.** The free-standing COF-PtaDha membrane was synthesized via acid-catalyzed interfacial polymerization of Pta and Dha. The Dha-ethyl acetate-mesitylene solution (5.0 mg, 0.03 mmol in 4 mL, V/V = 1/9) was gently placed on top of the phosphate-acetic acid aqueous solution (10.15 mg, 0.015 mmol in 4 mL of 3 M acetic acid solution). The system was kept at 35 °C for 3 d. The free-standing COF-PtaDha membrane was obtained after being washed thoroughly with water and acetone in sequence to remove any residual monomers and the catalyst, which was further rinsed with $H_2O$ for 24 h for permeation tests and air-dried for physicochemical characterization.

**Fabrication of the Free-Standing COF-PtaDha-$SO_3K$ Membrane.** The free-standing COF-PtaDha membrane was treated with 0.05 M KOH ethanol solution for 5 h and then washed thoroughly with ethanol. After that, the resulting membrane was soaked in a 0.05 M 1,3-propane sultone ethanol solution at 35 °C overnight. During this process, 1,3-propane sultone facilitated ring opening and the phenol oxygen anion nucleophilically attacked the $\alpha$ position of the sultone oxygen. This chemical transformation resulted in the incorporation of alkyl chains bearing terminal potassium-sulfonate groups ($-SO_3K$) into the pore channels of the membrane. The free-standing COF-PtaDha-$SO_3K$ membrane was obtained after being washed with water and acetone in sequence to remove any residual monomers and the catalyst, which was further rinsed with $H_2O$ for 24 h for permeation tests and air-dried for physicochemical characterization.

## ASSOCIATED CONTENT

### Supporting Information

The Supporting Information is available free of charge at https://pubs.acs.org/doi/10.1021/cbe.3c00119.

Experimental details, materials and characterization, monomer synthesis; tables of structure simulation, the dependence of Debye screening length on the concentration of KCl solutions, and osmotic energy harvesting performance comparison; FT-IR spectra, solid-state $^{13}C$ NMR spectrum, UV−vis spectrum, graphic of AA-stacking mode, device photos, $I-t$ and $I-V$ curves, IR camera images, $^1H$ NMR spectra, and additional ionic separation performance, SEM images, PXRD patterns, and $N_2$ sorption isotherms (PDF)

## AUTHOR INFORMATION


### Corresponding Author

**Qi Sun** − *Zhejiang Provincial Key Laboratory of Advanced Chemical Engineering Manufacture, Technology, College of Chemical and Biological Engineering, Zhejiang University, Hangzhou 310027, China;* orcid.org/0000-0002-1698-8741; Email: sunqichs@zju.edu.cn

### Authors

**Weipeng Xian** − *Zhejiang Provincial Key Laboratory of Advanced Chemical Engineering Manufacture, Technology, College of Chemical and Biological Engineering, Zhejiang University, Hangzhou 310027, China*

**Changjia Zhu** − *Department of Chemistry, University of North Texas, Denton, Texas 76201, United States;* orcid.org/0000-0002-6468-155X

**Zhuozhi Lai** − *Zhejiang Provincial Key Laboratory of Advanced Chemical Engineering Manufacture, Technology, College of Chemical and Biological Engineering, Zhejiang University, Hangzhou 310027, China*

**Qing Guo** − *Zhejiang Provincial Key Laboratory of Advanced Chemical Engineering Manufacture, Technology, College of Chemical and Biological Engineering, Zhejiang University, Hangzhou 310027, China*

**Di Wu** − *Zhejiang Provincial Key Laboratory of Advanced Chemical Engineering Manufacture, Technology, College of Chemical and Biological Engineering, Zhejiang University, Hangzhou 310027, China*

**Qing-Wei Meng** − *Zhejiang Provincial Key Laboratory of Advanced Chemical Engineering Manufacture, Technology, College of Chemical and Biological Engineering, Zhejiang University, Hangzhou 310027, China*

**Sai Wang** − *Zhejiang Provincial Key Laboratory of Advanced Chemical Engineering Manufacture, Technology, College of Chemical and Biological Engineering, Zhejiang University, Hangzhou 310027, China*

**Shengqian Ma** − *Department of Chemistry, University of North Texas, Denton, Texas 76201, United States;* orcid.org/0000-0002-1897-7069

Complete contact information is available at: https://pubs.acs.org/10.1021/cbe.3c00119

### Author Contributions

#W.X. and C.Z. contributed equally.


### Notes

The authors declare no competing financial interest.

## ACKNOWLEDGMENTS

This work was supported by the National Key Research and Development Program of China (2022YFA1503004), the National Science Foundation of China (22205198), and the National Science Foundation of Zhejiang province (LR23B060001, LY22B06004, and LY23B060022).

## REFERENCES


(1) Deutch, J. Is Net Zero Carbon 2050 Possible? *Joule* **2020**, *4*, 2237−2243.

(2) Zuo, X.; Zhu, C.; Xian, W.; Meng, Q.-W.; Guo, Q.; Zhu, X.; Wang, S.; Wang, Y.; Ma, S.; Sun, Q. Thermo-osmotic Energy Conversion Enabled by Covalent-organic-framework Membranes with Record Output Power Density. *Angew. Chem. Int. Ed.* **2022**, *61*, No. e202116910.

(3) Cai, J.; Ma, W.; Hao, C.; Sun, M.; Guo, J.; Xu, L.; Xu, C.; Kuang, H. Artificial Light-triggered Smart Nanochannels Relying on Optoionic Effects. *Chem.* **2021**, *7*, 1802−1826.

(4) Xie, X.; Bakker, E. Photoelectric Conversion Based on Photo-coupled Electron Transfer Reactions. *J. Am. Chem. Soc.* **2014**, *136*, 7857−7860.

(5) Lozada-Hidalgo, M.; Zhang, S.; Hu, S.; Kravets, V. G.; Rodriguez, F. J.; Berdyugin, A.; Grigorenko, A.; Geim, A. K. Giant Photoeffect in Proton Transport Through Graphene Membranes. *Nat. Nanotechnol.* **2018**, *13*, 300−303.

(6) Zhang, Z.; Wen, L.; Jiang, L. Nanofluidics for Osmotic Energy Conversion. *Nat. Rev. Mater.* **2021**, *6*, 622−639.

(7) Yang, J.; Hu, X.; Kong, X.; Jia, P.; Ji, D.; Quan, D.; Wang, L.; Wen, Q.; Lu, D.; Wu, J.; Jiang, L.; Guo, W. Photo-induced Ultrafast Active Ion Transport Through Graphene Oxide Membranes. *Nat. Commun.* **2019**, *10*, 1171.

(8) Zhu, C.; Zuo, X.; Xian, W.; Guo, Q.; Meng, Q.-W.; Wang, S.; Ma, S.; Sun, Q. Integration of Thermoelectric Conversion with Reverse Electrodialysis for Mitigating Ion Concentration Polarization and Achieving Enhanced Output Power Density. *ACS Energy Lett.* **2022**, *7*, 2937−2943.

(9) Xie, X.; Bakker, E. Creating Electrochemical Gradients by Light: From Bio-inspired Concepts to Photoelectric Conversion. *Phys. Chem. Chem. Phys.* **2014**, *16*, 19781−19789.
(10) Xiong, Y.; Liao, Q.; Huang, Z.; Huang, X.; Ke, C.; Zhu, H.; Dong, C.; Wang, H.; Xi, K.; Zhan, P.; Xu, F.; Lu, Y. Ultrahigh Responsivity Photodetectors of 2D Covalent Organic Frameworks Integrated on Graphene. *Adv. Mater.* **2020**, *32*, No. 1907242.
(11) Podjaski, F.; Lotsch, B. V. Optoelectronics Meets Optoionics: Light Storing Carbon Nitrides and Beyond. *Adv. Energy Mater.* **2021**, *11*, No. 2003049.
(12) Xiao, K.; Jiang, L.; Antonietti, M. Ion Transport in Nanofluidic Devices for Energy Harvesting. *Joule* **2019**, *3*, 2364−2380.
(13) Hong, S.; Zou, G.; Kim, H.; Huang, D.; Wang, P.; Alshareef, H. N. Photothermoelectric Response of $Ti_3C_2T_x$ MXene Confined Ion Channels. *ACS Nano* **2020**, *14*, 9042−9049.
(14) Zhang, Y.; Li, F.; Kong, X.; Xue, T.; Liu, D.; Jia, P.; Wang, L.; Ding, L.; Dong, H.; Lu, D.; Jiang, L.; Guo, W. Photoinduced Directional Proton Transport Through Printed Asymmetric Graphene Oxide Superstructures: A New Driving Mechanism under Full-area Light Illumination. *Adv. Funct. Mater.* **2020**, *30*, No. 1907549.
(15) Ling, H.; Xin, W.; Qian, Y.; He, X.; Lang, Y.; Chen, W.; Wu, Y.; Du, H.; Liu, Y.; Kong, X.-Y.; Jiang, L.; Wen, L. Heterogeneous Electrospinning Nanofiber Membranes with pH-regulated Ion Gating for Tunable Osmotic Power Harvesting. *Angew. Chem. Int. Ed.* **2023**, *62*, No. e202212120.
(16) Jia, P.; Wang, L.; Zhang, Y.; Yang, Y.; Jin, X.; Zhou, M.; Quan, D.; Jia, M.; Cao, L.; Long, R.; Jiang, L.; Guo, W. Harnessing Ionic Power from Equilibrium Electrolyte Solution via Photoinduced Active Ion Transport Through van-der-Waals-like Heterostructures. *Adv. Mater.* **2021**, *33*, No. 2007529.
(17) Wang, L.; Wen, Q.; Jia, P.; Jia, D.; Sun, X.; Jiang, L.; Guo, W. Light-driven Active Proton Transport through Photoacid- and Photobase-doped Janus Graphene Oxide Membranes. *Adv. Mater.* **2019**, *31*, No. 1903029.
(18) Cheng, B.; Zhong, Y.; Qiu, Y.; Vaikuntanathan, S.; Park, J. Giant Gateable Osmotic Power Generation from A Goldilocks Two-dimensional Polymer. *J. Am. Chem. Soc.* **2023**, *145*, 5261−5269.
(19) Yip, N. Y.; Brogioli, D.; Hamelers, H. V. M.; Nijmeijer, K. Salinity Gradients for Sustainable Energy: Primer, Progress, and Prospects. *Environ. Sci. Technol.* **2016**, *50*, 12072−12094.
(20) Cao, L.; Chen, I.-C.; Chen, C.; Shinde, D. B.; Liu, X.; Li, Z.; Zhou, Z.; Zhang, Y.; Han, Y.; Lai, Z. Giant Osmotic Energy Conversion through Vertical-aligned Ion-permselective Nanochannels in Covalent Organic Framework Membranes. *J. Am. Chem. Soc.* **2022**, *144*, 12400−12409.
(21) Safaei, J.; Gao, Y.; Hosseinpour, M.; Zhang, X.; Sun, Y.; Tang, X.; Zhang, Z.; Wang, S.; Guo, X.; Wang, Y.; Chen, Z.; Zhou, D.; Kang, F.; Jiang, L.; Wang, G. Vacancy Engineering for High-efficiency Nanofluidic Osmotic Energy Generation. *J. Am. Chem. Soc.* **2023**, *145*, 2669−2678.
(22) Gao, M.; Zheng, M.-J.; EL-Mahdy, A. F.; Chang, C.-W.; Su, Y.-C.; Hung, W.-H.; Kuo, S.-W.; Yeh, L.-H. A Bioinspired Ionic Diode Membrane Based on Sub-2 nm Covalent Organic Framework Channels for Ultrahigh Osmotic Energy Generation. *Nano Energy* **2023**, *105*, No. 108007.
(23) Chu, C.-W.; Fauziah, A. R.; Yeh, L.-H. Optimizing Membranes for Osmotic Power Generation. *Angew. Chem. Int. Ed.* **2023**, *62*, No. e202303582.
(24) Huang, K.-T.; Hung, W.-H.; Su, Y.-C.; Tang, F.-C.; Linh, L. D.; Huang, C.-J.; Yeh, L.-H. Zwitterionic Gradient Double-network Hydrogel Membranes with Superior Biofouling Resistance for Sustainable Osmotic Energy Harvesting. *Adv. Funct. Mater.* **2023**, *33*, No. 2211316.
(25) Fauziah, A. R.; Yeh, L.-H. Engineered Heterogenous Subnanochannel Membranes with A Tri-continuous Pore Structure of Large Geometry Gradient for Massively Enhanced Osmotic Power Conversion from Organic Solutions. *Adv. Funct. Mater.* **2024**, *34*, No. 2306834.
(26) White, W.; Sanborn, C. D.; Reiter, R. S.; Fabian, D. M.; Ardo, S. Observation of Photovoltaic Action from Photoacid-modified Nafion Due to Light-driven Ion Transport. *J. Am. Chem. Soc.* **2017**, *139*, 11726−11733.
(27) White, W.; Sanborn, C. D.; Fabian, D. M.; Ardo, S. Conversion of Visible Light into Ionic Power Using Photoacid-dye-sensitized Bipolar Ion-exchange Membranes. *Joule* **2018**, *2*, 94−109.
(28) Wei, S.; Zhang, F.; Zhang, W.; Qiang, P.; Yu, K.; Fu, X.; Wu, D.; Bi, S.; Zhang, F. Semiconducting 2D Triazine-cored Covalent Organic Frameworks with Unsubstituted Olefin Linkages. *J. Am. Chem. Soc.* **2019**, *141*, 14272−14279.
(29) Kandambeth, S.; Dey, K.; Banerjee, R. Covalent Organic Frameworks: Chemistry Beyond the Structure. *J. Am. Chem. Soc.* **2019**, *141*, 1807−1822.
(30) Jin, Y.; Hu, Y.; Zhang, W. Tessellated Multiporous Two-dimensional Covalent Organic Frameworks. *Nat. Rev. Chem.* **2017**, *1*, 0056.
(31) Guan, X.; Chen, F.; Fang, Q.; Qiu, S. Design and Applications of Three Dimensional Covalent Organic Frameworks. *Chem. Soc. Rev.* **2020**, *49*, 1357−1384.
(32) Geng, K.; He, T.; Liu, R.; Dalapati, S.; Tan, K. T.; Li, Z.; Tao, S.; Gong, Y.; Jiang, Q.; Jiang, D. Covalent Organic Frameworks: Design, Synthesis, and Functions. *Chem. Rev.* **2020**, *120*, 8814−8933.
(33) Ma, T.; Kapustin, E. A.; Yin, S. X.; Liang, L.; Zhou, Z.; Niu, J.; Li, L.-H.; Wang, Y.; Su, J.; Li, J.; Wang, X.; Wang, W. D.; Wang, W.; Sun, J.; Yaghi, O. M. Single-crystal X-ray Diffraction Structures of Covalent Organic Frameworks. *Science* **2018**, *361*, 48−52.
(34) Zhang, P.; Chen, S.; Zhu, C.; Hou, L.; Xian, W.; Zuo, X.; Zhang, Q.; Ma, S.; Sun, Q. Covalent Organic Framework Nanofluidic Membrane as A Platform for Highly Sensitive Bionic Thermosensation. *Nat. Commun.* **2021**, *12*, 1844.
(35) Meng, Q.-W.; Wu, S.; Liu, M.; Guo, Q.; Xian, W.; Zuo, X.; Wang, S.; Yin, H.; Ma, S.; Sun, Q. Guanidinium-based Covalent Organic Framework Membrane for Single-acid Recovery. *Sci. Adv.* **2023**, *9*, No. eadh0207.
(36) Guo, Q.; Lai, Z.; Zuo, X.; Xian, W.; Wu, S.; Zheng, L.; Dai, Z.; Wang, S.; Sun, Q. Photoelectric Responsive Ionic Channel for Sustainable Energy Harvesting. *Nat. Commun.* **2023**, *14*, 6702.
(37) Pachfule, P.; Acharjya, A.; Roeser, J.; Langenhahn, T.; Schwarze, M.; Schomäcker, R.; Thomas, A.; Schmidt, J. Diacetylene Functionalized Covalent Organic Framework (COF) for Photocatalytic Hydrogen Generation. *J. Am. Chem. Soc.* **2018**, *140*, 1423−1427.
(38) Zhang, M.; Lang, Z.-L.; Liu, J.; Chang, J.-N.; Li, L.-Y.; Shang, L.-J.; Wang, M.; Li, S.-L.; Lan, Y.-Q. Semiconductor-covalent Organic Framework Z-scheme Heterojunctions for Artificial Photosynthesis. *Angew. Chem. Int. Ed.* **2020**, *59*, 6500−6506.
(39) Keller, N.; Bein, T. Optoelectronic Processes in Covalent Organic Frameworks. *Chem. Soc. Rev.* **2021**, *50*, 1813−1845.
(40) Qian, Y.; Li, D.; Han, Y.; Jiang, H.-L. Photocatalytic Molecular Oxygen Activation by Regulating Excitonic Effects in Covalent Organic Frameworks. *J. Am. Chem. Soc.* **2020**, *142*, 20763−20771.
(41) Yang, S.; Hu, W.; Zhang, X.; He, P.; Pattengale, B.; Liu, C.; Cendejas, M.; Hermans, I.; Zhang, X.; Zhang, J.; Huang, J. 2D Covalent Organic Frameworks as Intrinsic Photocatalysts for Visible Light-driven $CO_2$ Reduction. *J. Am. Chem. Soc.* **2018**, *140*, 14614−14618.
(42) Chang, J.-N.; Li, Q.; Shi, J.-W.; Zhang, M.; Zhang, L.; Li, S.; Chen, Y.; Li, S.-L.; Lan, Y.-Q. Oxidation-reduction Molecular Junction Covalent Organic Frameworks for Full Reaction Photosynthesis of $H_2O_2$. *Angew. Chem. Int. Ed.* **2023**, *62*, No. e202218868.
(43) Zhou, T.; Wang, L.; Huang, X.; Unruangsri, J.; Zhang, H.; Wang, R.; Song, Q.; Yang, Q.; Li, W.; Wang, C.; Takahashi, K.; Xu, H.; Guo, J. PEG-stabilized Coaxial Stacking of Two-dimensional Covalent Organic Frameworks for Enhanced Photocatalytic Hydrogen Evolution. *Nat. Commun.* **2021**, *12*, 3934.
(44) Colson, J. W.; Woll, A. R.; Mukherjee, A.; Levendorf, M. P.; Spitler, E. L.; Shields, V. B.; Spencer, M. G.; Park, J.; Dichtel, W. R.

Oriented 2D Covalent Organic Framework Thin Films on Single-layer Graphene. *Science* **2011**, *332*, 228−231.
(45) Yuan, C.; Wu, X.; Gao, R.; Han, X.; Liu, Y.; Long, Y.; Cui, Y. Nanochannels of Covalent Organic Frameworks for Chiral Selective Transmembrane Transport of Amino Acids. *J. Am. Chem. Soc.* **2019**, *141*, 20187−20197.
(46) Ying, Y.; Tong, M.; Ning, S.; Ravi, S. K.; Peh, S. B.; Tan, S. C.; Pennycook, S. J.; Zhao, D. Ultrathin Two-dimensional Membranes Assembled by Ionic Covalent Organic Nanosheets with Reduced Apertures for Gas Separation. *J. Am. Chem. Soc.* **2020**, *142*, 4472−4480.
(47) Khan, N. A.; Zhang, R.; Wu, H.; Shen, J.; Yuan, J.; Fan, C.; Cao, L.; Olson, M. A.; Jiang, Z. Solid-vapor Interface Engineered Covalent Organic Framework Membranes for Molecular Separation. *J. Am. Chem. Soc.* **2020**, *142*, 13450−13458.
(48) Zhao, Y.; Guo, L.; Gándara, F.; Ma, Y.; Liu, Z.; Zhu, C.; Lyu, H.; Trickett, C. A.; Kapustin, E. A.; Terasaki, O.; Yaghi, O. M. A Synthetic Route for Crystals of Woven Structures, Uniform Nanocrystals, and Thin Films of Imine Covalent Organic Frameworks. *J. Am. Chem. Soc.* **2017**, *139*, 13166−13172.
(49) Shinde, D. B.; Sheng, G.; Li, X.; Ostwal, M.; Emwas, A.-H.; Huang, K.-W.; Lai, Z. Crystalline 2D Covalent Organic Framework Membranes for High-flux Organic Solvent Nanofiltration. *J. Am. Chem. Soc.* **2018**, *140*, 14342−14349.
(50) Fu, J.; Das, S.; Xing, G.; Ben, T.; Valtchev, V.; Qiu, S. Fabrication of COF-MOF Composite Membranes and Their Highly Selective Separation of $H_2/CO_2$. *J. Am. Chem. Soc.* **2016**, *138*, 7673−7680.
(51) Li, Y.; Wu, Q.; Guo, X.; Zhang, M.; Chen, B.; Wei, G.; Li, X.; Li, S.; Ma, L. Laminater Self-standing Covalent Organic Framework Membrane with Uniformly Distributed Subnanopores for Ionic and Molecular Sieving. *Nat. Commun.* **2020**, *11*, 599.
(52) Sasmal, H. S.; Hader, A.; Kunjattu, H. S.; Dey, K.; Nadol, A.; Ajithkumar, T. G.; Bedaur, P. R.; Banerjee, R. Covalent Self-assembly in Two Dimensions: Connecting Covalent Organic Framework Nanospheres into Crystalline and Porous Thin Films. *J. Am. Chem. Soc.* **2019**, *141*, 20371−20378.
(53) Bing, S.; Xian, W.; Chen, S.; Song, Y.; Hou, L.; Liu, X.; Ma, S.; Sun, Q.; Zhang, L. Bio-inspired Construction of Ion Conductive Pathway in Covalent Organic Framework Membranes for Efficient Lithium Extraction. *Matter* **2021**, *4*, 2027−2038.
(54) Hou, L.; Xian, W.; Bing, S.; Song, Y.; Sun, Q.; Zhang, L.; Ma, S. Understanding the Ion Transport Behavior across Nanofluidic Membranes in Response to the Charge Variations. *Adv. Funct. Mater.* **2021**, *31*, No. 2009970.
(55) Sahabudeen, H.; Qi, H.; Ballabio, M.; Položij, M.; Olthof, S.; Shivhare, R.; Jing, Y.; Park, S.; Liu, K.; Zhang, T.; Ma, J.; Rellinghaus, B.; Rellinghaus, S.; Heine, T.; Bonn, M.; Cánovas, E.; Zheng, Z.; Kaiser, U.; Dong, R.; Feng, X. Highly Crystalline and Semiconducting Imine-based Two-dimensional Polymers Enabled by Interfacial Synthesis. *Angew. Chem. Int. Ed.* **2020**, *59*, 6028−6036.
(56) Zhao, S.; Jiang, C.; Fan, J.; Hong, S.; Mei, P.; Yao, R.; Liu, Y.; Zhang, S.; Li, H.; Zhang, H.; Sun, C.; Guo, Z.; Shao, P.; Zhu, Y.; Zhang, J.; Guo, L.; Ma, Y.; Zhang, J.; Feng, X.; Wang, F.; Wu, H.; Wang, B. Hydrophilicity Gradient in Covalent Organic Frameworks for Membrane Distillation. *Nat. Mater.* **2021**, *20*, 1551−1558.
(57) Wang, P.; Peng, Y.; Zhu, C.; Yao, R.; Song, H.; Kun, L.; Yang, W. Single-phase Covalent Organic Framework Staggered Stacking Nanosheet Membrane for $CO_2$-selective Separation. *Angew. Chem. Int. Ed.* **2021**, *60*, 19047−19052.
(58) Kandambeth, S.; Shinde, D. B.; Panda, M. K.; Lukose, B.; Heine, T.; Banerjee, R. Enhancement of Chemical Stability and Crystallinity in Porphyrin-containing Covalent Organic Frameworks by Intramolecular Hydrogen Bonds. *Angew. Chem. Int. Ed.* **2013**, *52*, 13052−13056.
(59) Lin, G.; Ding, H.; Chen, R.; Peng, Z.; Wang, B.; Wang, C. 3D Porphyrin-based Covalent Organic Frameworks. *J. Am. Chem. Soc.* **2017**, *139*, 8705−8709.
(60) Steinberg-Yfrach, G.; Liddell, P. A.; Hung, S.-C.; Moore, A. L.; Gust, D.; Moore, T. A. Conversion of Light Energy to Proton Potential in Liposomes by Artificial Photosynthetic Reaction Centres. *Nature* **1997**, *385*, 239−241.
(61) Liu, K.; Qi, H.; Dong, R.; Shivhare, R.; Addicoat, M.; Zhang, T.; Sahabudeen, H.; Heine, T.; Mannsfeld, S.; Kaiser, U.; Zheng, Z.; Feng, X. On-water Surface Synthesis of Crystalline, Few-layer Two-Dimensional Polymers Assisted by Surfactant Monolayers. *Nat. Chem.* **2019**, *11*, 994−1000.
(62) Qian, Y.; Li, D.; Han, Y.; Jiang, H.-L. Photocatalytic Molecular Oxygen Activation by Regulating Excitonic Effects in Covalent Organic Frameworks. *J. Am. Chem. Soc.* **2020**, *142*, 20763−20771.
(63) Hu, H.; Zhu, J.; Cao, L.; Wang, Z.; Gao, Y.; Yang, L.; Lin, W.; Wang, C. Light-driven Proton Transport across Liposomal Membranes Enabled by Janus Metal-organic Layers. *Chem.* **2022**, *8*, 450−464.
(64) Zhang, Y.; Yang, L.; Yang, Y.; Li, W.; Liu, B.; Jin, X.; Zhou, M.; Long, R.; Jiang, L.; Guo, W. Bidirectional Light-driven Ion Transport through Porphyrin Metal−organic Framework-based van der Waals Heterostructures via pH-induced Band Alignment Inversion. *CCS Chem.* **2022**, *4*, 3329−3341.
(65) Sun, Q.; Tang, Y.; Aguila, B.; Wang, S.; Xiao, F.-S.; Thallapally, P. K.; Al-Enizi, A. M.; Nafady, A.; Ma, S. Reaction Environment Modification in Covalent Organic Frameworks for Catalytic Performance Enhancement. *Angew. Chem., Int. Ed.* **2019**, *58*, 8670−8675.
(66) Wang, S.; Sun, Q.; Chen, W.; Tang, Y.; Aguila, B.; Pan, Y.; Zheng, A.; Yang, Z.; Wojtas, L.; Ma, S.; Xiao, F.-S. Programming Covalent Organic Frameworks for Photocatalysis: Investigation of Chemical and Structural Variations. *Matter* **2020**, *2*, 416−427.
(67) Esplandiu, M. J.; Reguera, D.; Romero-Guzmán, D.; Gallardo-Moreno, A. M.; Fraxedas, J. From Radial to Unidirectional Water Pumping in Zeta-potential Modulated Nafion Nanostructures. *Nat. Commun.* **2022**, *13*, 2812.


https://doi.org/10.1021/cbe.3c00119
*Chem Bio Eng.* 2024, 1, 461−468